ACS APPLIED MATERIALS & INTERFACES

Research Article

www.acsami.org

Importance of Substrate Functionality on the Adhesion and Debonding of a Pressure-Sensitive Adhesive under Water

Preetika Karnal,[†] Paul Roberts,[†] Stefan Gryska,[§] Courtney King,[†] Carlos Barrios,*[,§] and Joelle Frechette*[,†,‡]

[†]Chemical and Biomolecular Engineering Department and [‡]Hopkins Extreme Materials Institute, (HEMI), Johns Hopkins University, Baltimore, Maryland 21218, United States

[§]3M Company, 3M Center, Building 201-4N-01, St. Paul, Minnesota 55144-1000, United States

Supporting Information

ABSTRACT: We investigate the effect of an aqueous environment on the adhesion of a model acrylic pressure-sensitive adhesive (PSA) composed of 2-ethylhexyl acrylate-*co*-acrylic acid. We use probe-tack adhesion measurements accompanied by in situ imaging of the contact region during bonding and debonding. Within the probe-tack tests, we use both hydrophilic (piranha and plasma treatment) and hydrophobic (C_{18}-silanization) surface treatments to investigate the contribution of the probe's surface energy on the underwater adhesion. In examining contact formation in air and underwater, we find that the presence of water when contact is made leads to different modes of PSA relaxation and contact formation. For all probes investigated, the adhesive strength between the PSA and the probe decreases when measured underwater. Additionally, we observe that the presence of water during debonding has a more pronounced effect on the adhesive strength of the PSA when probed by a hydrophilic surface as opposed to a hydrophobic surface. Using fingering wavelength analysis, we estimate the surface energy of the PSA in situ and find that when submerged in water, the PSA has a significantly higher surface energy compared to in air. Therefore, combining the observation of different modes of contact formation, the increase in surface energy, and the importance of the surface energy of the probe, we suggest that the decrease in adhesive strength in water can be explained by the hydration of the PSA and by trapped water defects between the PSA and the probe.

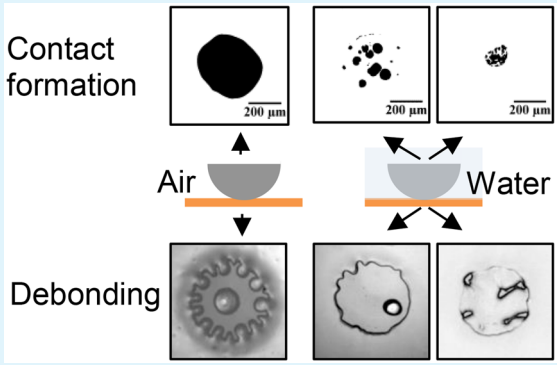

KEYWORDS: *adhesion, pressure-sensitive adhesive, acrylic, surface energy, probe-tack, water adsorption, fluid adhesion, underwater adhesion*

1. INTRODUCTION

Pressure-sensitive adhesives (PSAs) are a class of adhesives that bind to a substrate after a light external pressure has been applied. A PSA can be used effectively to bond on an array of surfaces with minimal applied pressure but can also be designed to be removed without leaving an adhesive residue.[1] PSAs are ubiquitous in everyday life (consider, for example, Scotch tape and Post-it notes), but they can also be found in electronics,[2,3] the automotive industry,[4] and in modern medical items such as wound dressings and drug delivery patches.[5] PSAs are also very intricate materials. They bear a mechanical load to maintain an adhesive bond and can sustain very large strains (>100%) prior to failure. The latter is a result from a unique characteristic of PSAs when compared to other adhesives, such as epoxies. During bonding, PSAs do not chemically react or change physically. In fact, unlike all other classes of adhesives, PSAs maintain their state as a soft, viscoelastic solid during both bonding and debonding.[6]

In contrast to the general understanding of the adhesion mechanisms of PSAs in air,[7] only a limited number of scientific reports address how the presence of water affects their performance. Most reports are on the effect of humidity rather than complete water immersion. Of note, Moon and Foster[8] showed that the degree of hydrophobicity of a PSA played an important role on its performance in humid environment. More specifically, they suggested that interaction of water molecules with the surface of a hydrophilic PSA lead to an increase in lateral forces with an increase in humidity. Recently, Schindler et al.[9] reported of probe-tack measurements on an acrylic PSA composed of 80% ethylhexyl acrylate and 20% methyl methacrylate (MMA), (poly(EHA-*stat*-20MMA), and performed X-ray reflectivity measurements at different relative humidities. Interestingly, they found that the failure mechanisms of the adhesive were altered upon increase in relative humidity, and reflectivity measurements indicated enrichment of methyl

Received: September 14, 2017
Accepted: November 6, 2017
Published: November 7, 2017

DOI: 10.1021/acsami.7b13984
ACS Appl. Mater. Interfaces 2017, 9, 42344−42353

methacrylate at the surface. They found that the maximum stress during debonding was independent of the relative humidity; however, the mode of failure changed from internal to external crack propagation with an increase in humidity.[8,9] In another recent study,[10] the surface structure of poly(butyl acrylate)-based pressure-sensitive adhesive was investigated during a drying process. Total internal reflection infrared (IR) absorption and visible−IR sum-frequency spectroscopies revealed that acrylic acid causes changes in the orientation of butyl acrylate at the surface due to favorable hydrogen bonding interactions with water. These precedents, while limited, demonstrate that a better understanding of the bonding and debonding mechanisms of PSAs in aqueous environments is needed and could lead to designing better adhesives, with a positive impact on extreme weather-resistant, medical, and surgical adhesives.[11]

There are multiple aspects of the adhesion between a PSA and a surface that could be affected by an aqueous environment. For efficient bonding under water, the fluid has to be displaced from the gap and crevices separating the surfaces. For example, visible−IR sum-frequency-generation spectroscopy (SFG) of the PDMS−sapphire interface suggests the presence of a heterogeneous contact region with trapped water pockets.[12] The SFG peaks indicate dangling −OH groups as well as water bands at the PDMS−sapphire interface in water. In addition, normal force measurements revealed lower adhesion for wet surfaces than dry surfaces. Defante et al.[13] has shown that in wet contact, rearrangement of a hydrophobic polymer coating at grain boundaries also led to trapped water in contact with a hydrophobic PDMS surface. Zhang et al.[14] also presented evidence of chemisorbed interfacial water in the contact region between a fused silica substrate and a film of poly(methyl silsesquioxane). Evidence suggests that water diffused through the interface rather than the bulk, forming hydrogen bonds with the polymer at the surface. Therefore, surface properties such as the wettability and roughness of both surfaces would play an important role in underwater adhesion.

The bulk viscoelastic properties of a PSA define its deformation and are the main contributors to their work of debonding.[15−21] As a result, any change in the bulk rheological properties of a PSA upon exposure to water will have important implications on adhesion. For example, fluid pockets can also be trapped during contact formation due to the deformation of a soft coating caused by viscous forces.[22−24] Additional experimental parameters are also expected to be important, such as the immersion time in water prior to contact with the probe, the dwell condition (time and load), and even the retraction velocity could cause drag and affect the measured adhesive properties. For example, the adhesive properties of acrylic PSAs adhered into polar substrates generally increase with longer contact times.[25,26] Part of this increase can be explained by an increase in contact area (true and nominal) between the PSA and the substrate over time due to the dynamic relaxation of the PSA as well as the reorganization within the PSA to increase the strength of the interface.[25,27,28] As a result, to characterize the underwater performance of PSAs, a better understanding of the individual contributions from the surface and the bulk properties are necessary, while it is nearly impossible to completely isolate the two contributions.

Here we show how (1) the presence of water during the bond-making step leads to different modes of contact formation and relaxation between the PSA and the probes and that (2) the presence of water leads to a more pronounced decrease in adhesion from a hydrophilic probe than from a hydrophobic one. The experiments are performed with an acrylic PSA (a cross-linked copolymer of 2-ethylhexyl acrylate and acrylic acid). Acrylic PSAs are common, and their performance and mechanisms for debonding in air are well-characterized, making them a good model system to study underwater adhesion. We perform adhesion measurements in the sphere−plane configuration where the interacting surfaces are completely submerged in water, and we can image the contact formation and debonding using an inverted microscope. In particular, we investigate how the wetting properties of the probe have a pronounced effect on the underwater performance of the PSA. Finally, we propose possible mechanisms to explain how water alters the adhesive properties of the PSA that are supported by our experimental results. To the best of our knowledge, this is the first report on the effect of how water affects the bond formation and adhesion of acrylic PSAs.

2. MATERIALS AND METHODS

2.1. Materials and Sample Preparation. *Solvent-Based PSA Synthesis.* Model pressure-sensitive adhesives based on copolymers of 2-ethylhexyl acrylate (2-EHA) and acrylic acid (AA) are prepared by radical polymerization. The monomers are mixed with ethyl acetate, as reaction solvent, at a concentration of 30 wt % and followed by the addition of VAZO 67, as thermal radical initiator, at a concentration of 0.3 wt % in amber, narrow necked pint bottles at room temperature. A benzophenone derivative (i.e 4-acryloyloxy benzophenone) is then added to be used as the photo-cross-linking agent. The solutions are deaerated by purging with nitrogen gas for 10 min and capped tightly before starting the polymerization. The bottles are immersed in a water bath (Launderometer, Atlas), where the polymerization is initiated and occurs at 60 °C with continued agitation for 24 h. After polymerization, bottles are cooled to room temperature, and the polymer solutions are used for solvent-based pressure-sensitive adhesives. PSA samples are then analyzed by conventional GPC against polystyrene molecular weight standards using THF as the solvent and eluent. A sample with a composition of 88 mol % of 2-ethylhexyl acrylate and 12 mol % of acrylic acid having a weight-average molecular weight (M_w) of 1 200 000 g/mol was selected for the totality of the results showed in this work. Table 1 summarizes the detailed GPC characterization of the PSA. An acrylic acid content of 12 mol % (5 wt %) was selected to represent common typical acrylic PSA.[29]

Table 1. Molecular Weight Result of Selected PSA[a]

	M_n g/mol	M_w g/mol	M_p g/mol	$Đ$
PSA	286 667	1 199 002	1 175 371	4

[a]Results are averages from duplicate injections. M_n = Number-average molecular weight, M_w = Weight-average molecular weight, M_p = Molecular weight at signal peak, $Đ$ = Dispersity = M_w/M_n (previously known as polydispersity index).

The PSA solutions are then coated on a release liner and dried in a convection oven at an average temperature of 150 °F, which is then followed by exposure to UV at a set total adsorbed dose of UV−B light = 400 mJ/cm^2 (directly measured using a power puck radiometer) using a processor from Fusion UV-systems for cross-linking, and then the adhesives between release liners are used as transfer tapes for further evaluation. Dry PSA films of thickness 25 μm are then transferred on PET release liner for adhesion testing. For rheology measurements, stacks of the same material are used.

PSA Sample Preparation. Circular glass coverslips are used as support substrates for the PSAs. Prior to the deposition of the PSA, the coverslips are cleaned via sonication in isopropanol followed by sonication in ethanol for 20 min each. They are then rinsed with ethanol and dried with nitrogen. Circular PSA-liner samples are cut from a larger sheet using a 25 mm punch and then deposited liner side

DOI: 10.1021/acsami.7b13984
ACS Appl. Mater. Interfaces 2017, 9, 42344−42353

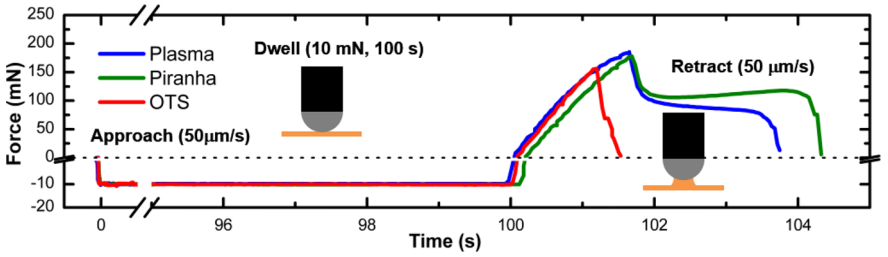

Figure 1. Typical force−time curves for the contact, dwell, and debonding of the acrylic PSA. The measurements are performed in air with a glass hemispherical probe. Measurements are performed with three different surface functionalizations for the glass probe: oxygen plasma (blue), piranha (green), and OTS (red). The applied load during dwell is 10 mN (for 100 s) and the retraction velocity is 50 μm/s. Compressive forces are negative.

up on clean circular coverslips. Prior to removing the liner, a 2 kg roller is used 20 times to roll over the PSA coverslips. The sample is then mounted on the multi-mode force microscope (see below) for testing. The PSA roughness on the coverslip is characterized by a confocal microscope (Keyence VK-X100).

Glass Probes. We use plano-convex (spherical) lenses with a radius of curvature R = 7.06 mm as probes for the tack measurements (Edmund Optics). Hydrophilic lenses are functionalized either by plasma treatment or piranha solution. The plasma-treated lenses are exposed to O_2 plasma for 5 s at 50 W in a homemade induction plasma reactor at 300 mTorr. For all experiments, the probes are used in a probe-tack test within 5 min of plasma treatment. Piranha-treated lenses are placed in piranha solution (1:3 volume ratio of H_2O_2 and H_2SO_4, respectively). Treated lenses are stored in water and used within 24 h after drying with nitrogen. Hydrophobic lenses are functionalized with OTS (octadecyltrichlorosilane, Sigma-Aldrich) via solution deposition. Prior to silanization, the lenses are plasma cleaned for 5 s. They are subsequently placed in a cleaned glass beaker in a solution consisting of 20 mL of toluene and 40 μL of OTS for 20 min. The lenses are then rinsed with toluene to remove excess OTS and dried at 100 °C for at least 30 min. Following drying, the hydrophobic lenses are stored in a covered dish and used within 24 h. The static contact angle of water after the silanization treatment with OTS was 109°.

2.2. Probe-Tack Measurements. *Multi-mode Force Microscope (MMFM).* Probe-tack measurements are performed with the MMFM, a custom-built normal and lateral force instrument.[30] In the MMFM, the forces are measured from the deflection of a cantilever spring that is mounted on a microtranslating stage. The cantilever has a spring constant of 4500 N/m, and deflection of the spring is monitored via a fiber optic probe. The substrates are located at the bottom of an aluminum bath mounted on an inverted microscope (Axiovert 135, Zeiss) equipped with a camera (Grasshopper3, Point Gray) allowing for imaging of the contact area. A custom-designed LabVIEW platform (National Instruments) collects the microtranslator position, cantilever deflection, and images with corresponding time stamps. Images were analyzed using ImageJ (NIH).

Experimental Protocol. A freshly functionalized lens is used for each probe-tack measurement. The PSA coverslips are immobilized by a circular locking screw that clamped the coverslip beneath a Viton O-ring in the fluid bath. During a probe-tack test, the microtranslator lowered the cantilever at a velocity of 50 μm/s until the cantilever applied a −10 mN normal force to the sample (negative here by convention). A force feedback loop made slight adjustments to the cantilever's position during the 100 s dwell to maintain a constant applied force (to within ±0.2 mN, see Figure S7 in the Supporting Information (SI)). After dwell, the cantilever retracted at 50 μm/s until complete debonding occurred. A dwell time of 100 s is chosen so that the PSA has sufficient time to relax: the contact area increases by less than 2% from 50 to 100 s in contact. The debonding speed (50 μm/s) is such that the strain rate (debonding speed/adhesive thickness: 2 s^{-1}) is comparable to other probe-tack tests.[31,32] We found 2 s^{-1} is also optimum in order to move fast enough while also obtaining the necessary debonding images to analyze. The applied load is such that we can observe a high confinement ratio while also a low enough contact pressure to favor debonding at the glass probe−PSA interface. The confinement ratio between the radius of the contact area and the adhesive film thickness is ∼10.[33] The contact pressure at the glass probe−PSA bond is ∼0.05 MPa, which is less than the applied contact pressure of ∼0.2 MPa that was applied on the glass coverslip−PSA bond. For the three probes, the mode of detachment is adhesive,[7,29] meaning that there are no PSA residues left on the probe after debonding. We replaced the probe with a freshly treated one between each measurement. Over the course of the entire probe-tack test, images are captured at 10 frames per seconds with a 5× microscope objective. The procedure for probe-tack tests in air and in water are identical, except water is placed on the sample and contained in the MMFM bath for tests in water. Deionized (DI) water of conductivity 18.2 MΩ obtained from a Milli-Q gradient system was used as is. The pH of the DI water was not controlled and could vary from pH 8 to 6. All adhesion measurements are repeated three times for each lens treatment (plasma, piranha, and OTS) and for each environmental condition (in air, 5 min water immersion, and 60 min water immersion). Measurements are performed at room temperature and at less than 50% relative humidity.

Image Analysis. Images obtained from the adhesion measurements are processed using ImageJ software. Contact and debonding images taken under water are shown after subtracting an initial out-of-contact background image. Images have also been converted into greyscale with some changes in brightness and contrast. For contact area calculation, we threshold the images to enhance the visibility of the contact area, followed by conversion into a binary image. The contact area is calculated by counting the total number of black (contact) pixels through Matlab and scaling the pixel area with the actual image area. Analysis of the fingering instabilities is performed via image analysis to estimate in situ surface energy of the PSA in water.

2.3. PSA Characterization. We characterized the bulk and surface properties of the PSA in air and after exposure to water. Details and interpretation of the characterization are available in the SI. In summary, dynamic contact angles measured in air did not show a significant change in the advancing surface energy of the PSA when measured after water immersion (see section 1 in the SI). However, underwater measurement of static contact angle of diiodomethane on annealed PSA showed an increase with immersion time in water (see the SI, Figure S1−2). We also imaged the PSA using a confocal microscope. Based on confocal imaging, we estimate the root-mean square (RMS) surface roughness of the PSA to be 3.4 μm (see the SI, Figure S2). Oscillatory rheology measurement also did not exhibit a significant change in the storage (G') or loss (G'') moduli after up to 4 h immersion in water (see the SI, Figure S3). Minimal variations upon exposure to water were observed in G', G'', and tan (δ), even at large strains. In situ ATR-IR measurements showed an increase in absorbance of water with time in the PSA caused by water absorption (see the SI: section 3 for detailed description and analysis and Figure S4). Based on the ATR-IR spectra, we obtain a diffusivity of 1.1 ± 0.2 × 10^{-9} cm^2/s based on both H−O−H scissor-bending and O−H stretching.

3. RESULTS AND DISCUSSION

3.1. Debonding in Air. We first perform probe-tack measurements in air to investigate how the surface treatment of the

DOI: 10.1021/acsami.7b13984
ACS Appl. Mater. Interfaces 2017, 9, 42344−42353

glass probe affects the debonding force. We rely on three different hemispherical glass probes: two are hydrophilic and one is hydrophobic. The hydrophilic probes are treated either with a piranha solution or with oxygen plasma. Both treatments are routinely employed to increase the surface energy of the treated glass surface such that it becomes completely wettable by water (contact angle <10°). Both oxygen plasma and piranha treatment results in hydroxylation[34−36] of the surface, creating silanol terminated surfaces. However, the surface density of such groups may vary between different treatments. We investigate both treatments to generalize our observations to the wettability of the probe rather than on a specific cleaning protocol. Contact is made with the acrylic PSA using the MMFM, and a −10 mN compressive load (negative here by convention and controlled via a feedback loop) is applied for 100 s dwell time (region with negative force in Figure 1). Then the probe retracts at 50 μm/s (2 s^{-1} strain rate) from the PSA surface (region of positive force in Figure 1).

We find that hydrophilic probes require higher forces to detach from the PSA than the hydrophobic probe when they are loaded under the same conditions (Figure 1). We also see that a plateau is observed past the maximum force (i.e., at large strains) during the detachment with the hydrophilic probes, whereas this plateau is absent for the hydrophobic probe. These observations are consistent with prior work studying the effect of surface functionality on probe-tack tests (and on adhesion in general). The lower maximum debonding force in air obtained with a hydrophobic probe is in part due to lesser difference of the surface free energy between the hydrophobic probe and PSA than the hydrophilic probe and PSA.[37] Fibrillation of the PSA when in contact with a hydrophilic probe explains the presence of the plateau past the peak force. There is an empirical relationship relying on the rheological properties employed to predict the presence of a plateau at large strain.[38] The relationship states that a plateau is observed only when tan $\delta(\omega)/G'(\omega)$ is larger than a critical value that depends on a given PSA as well as on the surface−surface interactions. This critical value increases as the surface energy of probe decreases. Therefore, it is possible that the tan $\delta(\omega)/G'(\omega)$ value for the acrylic adhesive employed here (1.7×10^{-5} Pa^{-1}) is large enough to exhibit a plateau at higher strains when bonded to a higher surface energy substrate (hydrophilic probe). However, an even higher value would be required for a lower surface energy substrate (hydrophobic probe) to exhibit the plateau. Thus, the reduction in surface energy of the probe would be sufficient for the plateau to not be observed, which is in qualitative agreement with a previous study.[38]

3.3. Debonding in Water. We investigate how the detachment forces for the three probes change when measured in water. For these measurements, the PSA is first submerged in water in the liquid bath of the MMFM for an immersion time of either 5 or 60 min. During the water immersion period, the probes are kept in air and only immersed in water during approach to make contact with the PSA. After immersion, the probe makes contact and detaches following the same protocol as for the measurements in air. The hydrodynamic force is about 16.2 μN at a separation of 2.5 μm, which is close to the roughness of PSA film. This force is much smaller than our contact force of 10 mN, and hence, the drag of the cantilever during the approach does not contribute significantly to the forces measured underwater. As for measurements in air, the mode of failure of the PSA is always adhesive. We find that detachment in water leads to a significant decrease in the overall maximum detachment forces for the three probes investigated (Figure 2). The decrease of the maximum detachment

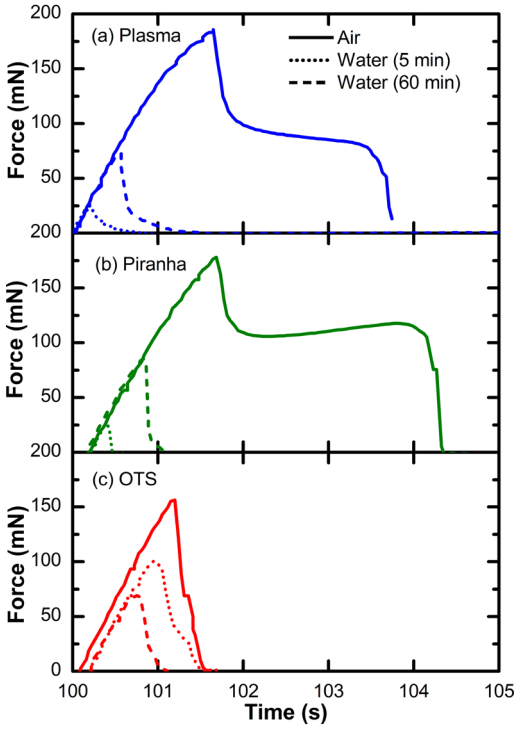

Figure 2. Effect of water on the detachment force from the PSA. The force−time plots are measured after identical dwell conditions (100 s at 10 mN) and identical retraction rate (50 μm/s). Measurements in water are taken after the PSA has been immersed in water for 5 min (dotted lines) and 60 min (dashed lines). Curves show the debonding forces for glass probes treated with (a) oxygen plasma, (b) piranha, and (c) OTS. The mode of failure is adhesive for all conditions investigated.

force (peak force) is more pronounced when contact is made with the hydrophilic probes than with the hydrophobic one. For the hydrophilic probes, in addition to the decrease in the maximum debonding force, the plateau at high strain also disappears in water. Note here that the tan $\delta(\omega)/G'(\omega)$ is constant for the measurements; therefore, the loss of the plateau at high strain is indicative of a change in surface−surface interaction. The immersion time of the PSA prior to contact with the probe also has an effect on the detachment force. In the case of the hydrophobic probe, a longer exposure to water leads to a steady decrease in the maximum debonding force (Figure 2b). In contrast, for the hydrophilic probes, we observe a small but significant increase in the maximum debonding force for a longer water immersion time (Figure 2a).

While the loading conditions and dwell time are the same for all the probe-tack measurements, the contact area between the PSA and the probe could be different for the different probes or environmental conditions. A significantly different contact area could explain the decrease in the detachment force in water. We monitor the contact radius during dwell using an inverted microscope (see Figure 3). We find that after dwell, the contact area is 4−8% larger with the hydrophobic probe than with the hydrophilic probe. We also observe that exposure to water leads to a systematic reduction of the contact area by ∼14% with all three probes. We also note that a longer exposure to water leads to a further reduction in the contact area for contact with

DOI: 10.1021/acsami.7b13984
ACS Appl. Mater. Interfaces 2017, 9, 42344−42353

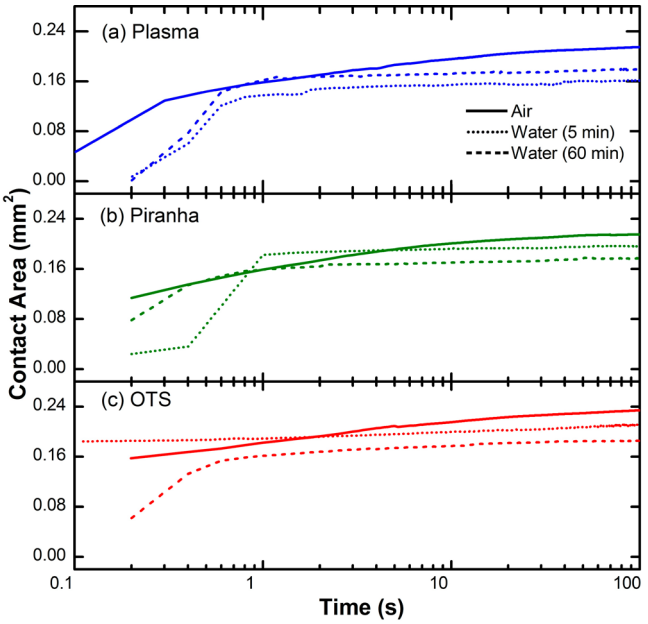

Figure 3. Growth of the nominal contact area between the probe and the PSA during dwell at 10 mN in air (solid lines) and when contact is made after (dotted lines) 5 min and (dashed lines) 60 min immersion of the PSA in water. The relaxation during dwell is under a 10 mN compressive load for all cases. Curves show the contact area for glass probes treated with (a) oxygen plasma, (b) piranha, and (c) OTS.

the hydrophobic probe. In contrast, we find that the contact area with a plasma-treated probe increases slightly when the PSA has been immersed in water for 60 min compared to 5 min prior to contact formation.

We find that the initial probe–PSA contact formation and relaxation is drastically different when contact is made in water compared to contact made in air (see Figure 4). Imaging of the

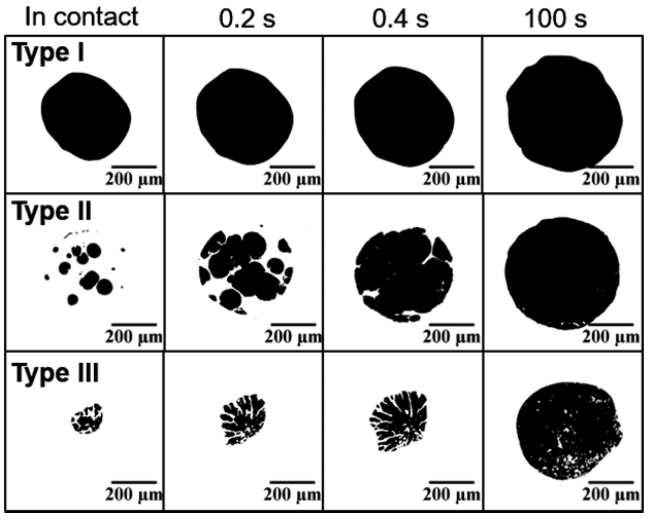

Figure 4. Bonding images of PSA showing three types of contact mechanisms. Type I is homogeneous contact formation. Type II has circular contact spots that merge with time. Type III shows dispersed contact that grows over time.

"wetting out phase" (relaxation) under a constant load during dwell shows three different morphologies for contact relaxation (Figure 4). A homogeneous (uniform) contact formation (Type I in Figure 4) is observed for all the PSA–probe contacts in air. In contrast, the PSA bonds with the probes in a very different fashion in water (Type II and Type III in Figure 4). Initial contact formation and growth can either start forming circular contact spots that grow and merge with time (Type II). Alternatively, we also observe a contact area that is more dispersed or fractal as it grows during dwell (Type III). We find that bonding with a hydrophobic probe is always of Type II, whereas hydrophilic probes may bond by either Type II or Type III contact. Contact with the piranha-treated probe is split nearly evenly between Type II and Type III. For the plasma-treated probes, there is a slight preference for Type III contact formation. Note that it is possible that Type II or Type III contact formation occurs also in air but that the dynamics are much faster than the image acquisition rate in our experiments (faster image acquisition rate in air, also does not show heterogeneous contact within the first 1 ms).

Contact relaxation via Type II or Type III could favor the presence of microscale trapped water pockets in the contact region prior to debonding between the PSA and the probe. It is also possible that drainage and lubrication forces during the approach to contact cause deformation of the PSA, leading to the nonuniform contact formation.[23,24,39] For example, a rough estimate of the deformation prior to contact based on the "offset contact deformation" in ref 22 is 0.5 μm. The observed heterogeneous contact formation in water is similar to what was predicted in ref 12, although the wetting properties of the interacting surfaces are different. These trapped water defects could reduce the true contact area of the PSA–probe and also act as defects for crack nucleation. However, we find that after the 100 s dwell time, the difference between true and nominal contact areas is small; for example, the maximum contact area of PSA in water decreased from 0.170 to 0.168 mm^2 when considering the trapped water defects as noncontact regions. Note here that our resolution limit for this magnification is 1.2 μm and that water pockets smaller than 1.44 μm^2 would be almost impossible to detect but could still be present. In addition, our measurements cannot detect adsorbed water at a molecular level between the PSA and the probe.

PSAs may exhibit different dissipation mechanisms such as fingering[7,40,41] and cavitation[7,42] prior to debonding fully from the probe. Alternatively, PSAs can debond only by external crack propagation[9,43] without any fingering or cavitation. In general, a weaker bond with the probe can lead to external crack propagation. In our experiments, PSA probed in air always debonds through fingering and cavitation. Cavitation appears before fingering for the hydrophobic probe, whereas fingering features are formed before cavitation for the hydrophilic probe. When surrounded by water and approached by the hydrophobic probe, the PSA continues to debond via cavitation and fingering (Figure 5). However, when approached by a hydrophilic probe in water, the PSA debonds through external crack propagation (Figure 6). The presence of water, either as trapped pockets or adsorbed at the PSA–water interface, could weaken the bond with the probe and lead to external crack propagation.

We can approximate the in situ change in surface energy of the PSA based on the spacing between the fingers during detachment.[40,44,45] For viscoelastic solids, the presence of fingers during detachment is indicative of a classic Saffman–Taylor instability.[40,44,45] Previous studies used linear stability analysis to show that the fingering wavelength, λ, is directly related to the surface energy of the material, γ (here PSA–air or

DOI: 10.1021/acsami.7b13984
ACS Appl. Mater. Interfaces 2017, 9, 42344–42353

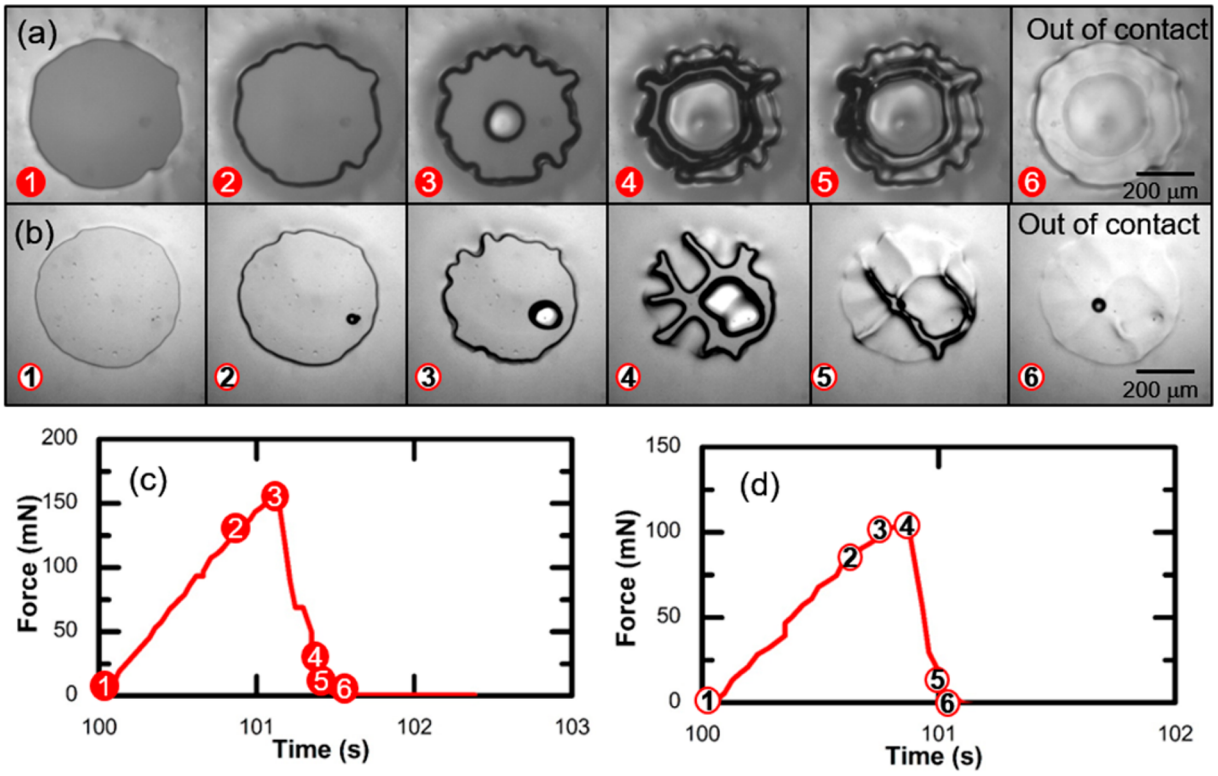

Figure 5. Sequence of debonding images of PSA probed by hydrophobic substrate along with force curves. PSA is in an air (filled circles: a,c) or water environment (open circles: b,d). PSA debonds via fingering and cavitation in both environments for the hydrophobic probe.

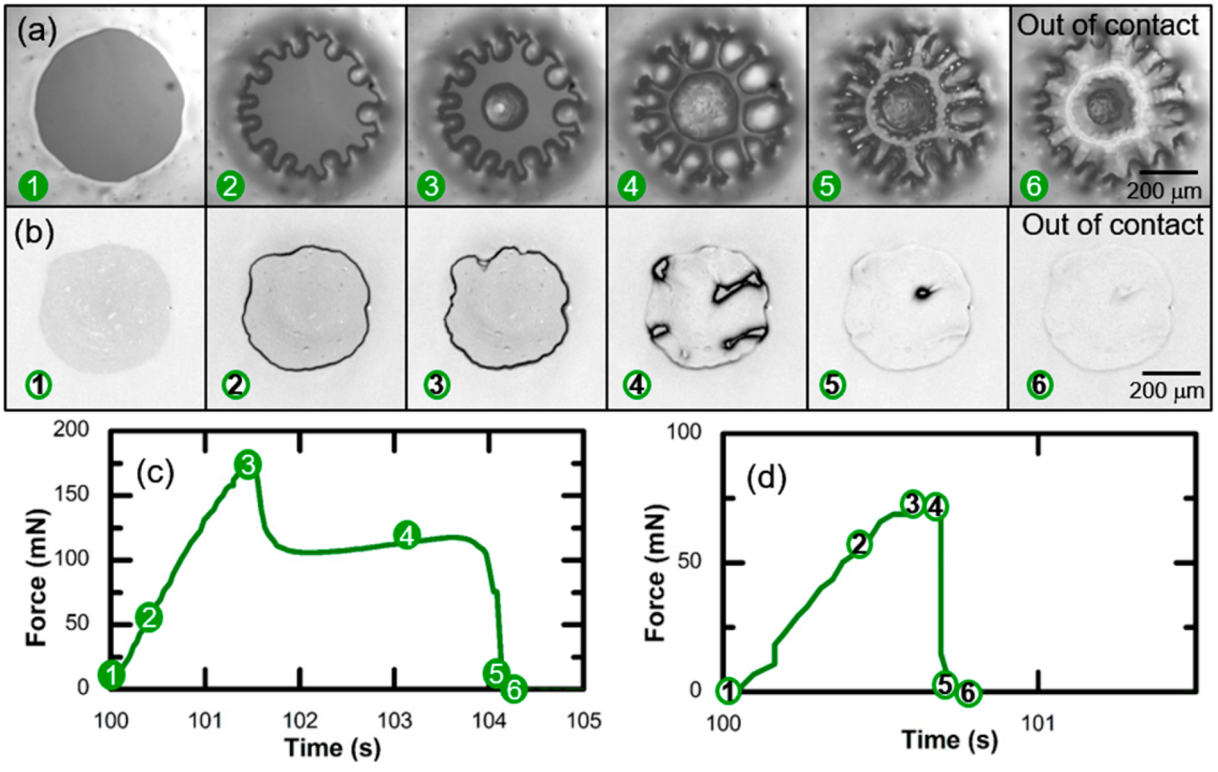

Figure 6. Sequence of debonding images of PSA probed by hydrophilic substrate along with force curves. PSA is in an air (filled circles: a,c) or water (open circles: b,d) environment. PSA debonds via fingering and cavitation in air and through external crack propagation in water.

PSA−water) exhibiting these features via eq 1

$$\lambda = \frac{\pi L}{\sqrt{\left(\frac{U\eta}{\gamma}\right)}} \quad (1)$$

where L is the thickness of the PSA, U is the radial velocity of the fingers, and η is the viscosity of the PSA. Therefore, based on eq 1, we find that for the same adhesive (thickness, viscosity), we have

DOI: 10.1021/acsami.7b13984
ACS Appl. Mater. Interfaces 2017, 9, 42344−42353

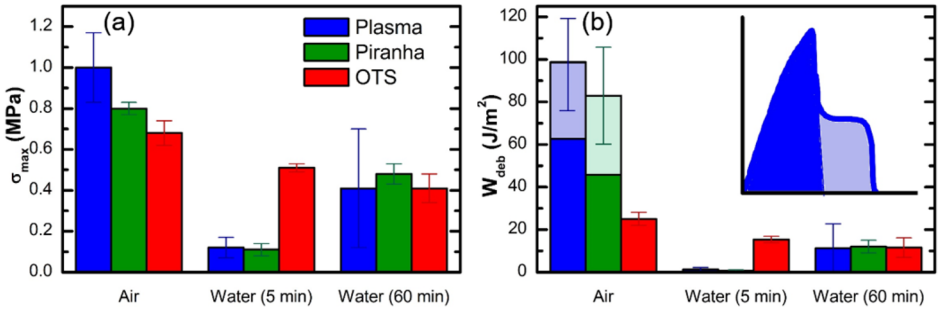

Figure 7. (a) Maximum debonding stress and (b) work of debonding of acrylic PSA in air and in water (5 and 60 min immersion time). The glass probe is functionalized by oxygen plasma, piranha, or OTS. For measurements in air with hydrophilic probe, lighter regions represent work associated with plateau formation as shown in the inset.

$$\sqrt{\gamma} \propto \lambda\sqrt{U} \tag{2}$$

Thus, we can use eq 2 as an attempt to obtain direct in situ estimates of the change in surface energy of the PSA after immersion in water (5 min water and 60 min water). Note here that we estimate the change in the PSA surface energy and not of the PSA−probe bond energy from this method. Saffman−Taylor instabilities occur when a less viscous fluid (here air or water) is "injected" into a more viscous one (here the PSA). The difference in viscosities is the cause of the instability. As a result, this analysis should lead to the same finger wavelength, independent of the strength of the PSA−probe interface (as long as the strength is high enough to cause finger in the first place). However, the analysis does not account for other mode of dissipation, such as cavitation, so it is only approximate here.

Based on fingering analysis, we observe a significant increase in the surface energy of the PSA upon exposure to water (see details of the analysis as well as all the numerical values in section 3 of the SI). From eq 2, we find that the surface energy increases from 12.2 to 25.8 ± 10.0 mJ/m^2 after 5 min water immersion. It further increases to 28.1 ± 12.0 mJ/m^2 at 60 min water immersion. These values are calculated from image analysis to obtain the finger wavelength and radial velocity. We then use the surface free energy of the PSA measured in air obtained from contact angle measurements as a reference state (Table S1) to cancel the material properties (L and η). Based on this approximation, the increase in surface energy in water is significant and likely due to a reconfiguration at the PSA−water interface that exposes more acrylic acid groups.[9] An increase in the surface energy of the PSA would favor wetting with water and could hinder water removal during contact formation, especially with a hydrophilic probe.

3.4. Mechanism for the Effect of Water on PSA Adhesion. We combine the contact area at the end of dwell with the debonding curve of Figure 2 to calculate the maximum debonding stress and the work of debonding (see Figure 7). The maximum debonding stress is calculated by normalizing the maximum debonding force by the maximum contact area before detachment. The work of debonding is calculated by integrating the area under the force−displacement curve (where displacement is the normal displacement of the probe−PSA interface caused by both cantilever motion and deflection) and normalizing it with the maximum area before detachment (obtained from image analysis). The maximum stress and work of debonding eliminate the contribution originating from the different nominal contact areas prior to detachment. As seen in Figure 7, it is clear that the effect of the probe treatment and water immersion are still important, and the same trends shown in Figure 2 are present in the maximum debonding stress and work of debonding. For instance, we can readily see that debonding in water always reduces the maximum stress and the work of detachment. We also observe that immersion time has an opposite effect if the probe is hydrophilic or hydrophobic. Finally, we also highlight in Figure 7 the fraction of the work of debonding that originates from the large strain plateau region and the one that originates from the detachment work prior to the peak force (shaded region and inset of Figure 7b). We see that the decrease in adhesion between a hydrophilic and a hydrophobic probe in air is mainly due to the disappearance of the plateau, but the decrease in the maximum stress cannot be neglected. We could not find a relationship between the peak stress or work of debonding and the mode of contact formation (Type II or Type III in Figure 4).

Because the bulk properties of the PSA are not affected by immersion in water under the conditions reported here (25 μm films, up to 4 h immersion time), the role of water on the debonding stress can be mainly understood in terms of change in interfacial properties. Note we only address below the surface energy (conservative) aspect of the PSA adhesion and not the dissipative (bulk viscoelastic deformation) ones. We also ignore possible change of the rheological properties that would only occur at the interface and not be measurable from bulk measurements. First, we can estimate the thermodynamic work of adhesion in air for our system using the Girifalco−Good eq (eq 3),[46,47] which relates work of adhesion (W_{12}) with the surface free energies of the two surfaces where the treated glass probe is denoted by (1) and the PSA by (2) (see Figure 8a).

$$|W_{12}| = 2\sqrt{\gamma_1\gamma_2} \tag{3}$$

Eq 3 estimates the work of adhesion of the PSA detached from a treated probe in air by considering only disperse (van der Waals) components (it ignores contributions from other conservative forces such as hydrogen bonding, for example). Nondisperse components could be present due to the acrylic acid in the PSA and the reactivity of the hydrophilic probes after treatment. However, consideration of nondisperse components are likely to further increase the W_{12} for the hydrophilic probe. If we compare the work of adhesion in air for the PSA bonded to a hydrophilic versus a hydrophobic probe, eq 3 predicts a larger W_{12} for the hydrophilic probe because of its higher surface energy (γ_1), which is what we observe in our experiments.

We then consider how introducing water as the medium (noted as subscript 3, see Figure 8) would affect the thermodynamic work of adhesion. van der Waals interactions always decrease when the dielectric of the medium increases (here going

DOI: 10.1021/acsami.7b13984
ACS Appl. Mater. Interfaces 2017, 9, 42344−42353

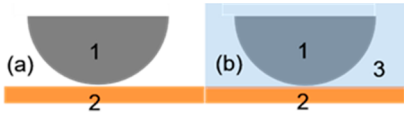

Figure 8. Schematic of glass lens bonded to the PSA surface in (a) air and (b) water for probe-tack measurements. The subscripts for the surface energies in the text are illustrated where (1) is glass probe, (2) is the PSA, (3) is water medium.

from air to water). Therefore, we expect that the work of adhesion would decrease when the measurements are performed in water, regardless of the probe. In addition, because glass and hydrocarbons (OTS) have similar dielectric spectra, we would expect a similar decrease in adhesion for measurements in water with a hydrophilic or hydrophobic probe.[47] Our experiments indeed show that both W_{deb} and σ_{max} decrease in water. However, we find that a water environment leads to a more significant decrease in W_{deb} and σ_{max} with the hydrophilic probe than with the hydrophobic probe. Such a difference is unlikely to be explained by solely changing the medium from air to water in the thermodynamic work of adhesion alone based only on dispersive components. Because W_{deb} and σ_{max} are normalized with the contact area, their reduction in water is also unlikely to be due to the relatively small changes in the nominal contact areas after dwell.

We suspect that more water is trapped in the PSA–hydrophilic probe contact region than when the probe is hydrophobized with an OTS layer. Keeping water in the contact region, either adsorbed or trapped at defects, would be more favorable with a hydrophilic probe. Such trapped water would act as a site for crack nucleation and could lead to an additional decrease in the maximum stress or work of debonding. Imaging of the contact area during debonding supports this hypothesis. When contact is made in water with the hydrophilic probes, we observe that the mode of failure is external crack propagation. Specifically looking at external crack propagation on the debonding PSA from the hydrophilic substrate in water, we find that crack propagation advances more quickly at regions with a higher density of water pocket defects. In contrast, the mode of debonding with the hydrophobic probe in water remains fingering and cavitation. Moreover, based on the analysis of the finger wavelengths we find that the PSA–water surface energy increases in water, which would make it more favorable to trap water during contact formation. At a molecular level, adsorbed water would also lead to a weakening of the probe–PSA interface bond. The adsorbed water would be easier to displace during contact with a hydrophobic probe than with a hydrophilic one.[13]

To confirm the role of trapped and/or adsorbed water, we performed additional experiments where contact between a hydrophilic probe and the PSA is made in air, followed by addition of water in the bath 45 s before detachment (Figure 9). We observe a decrease in both the maximum force and work of debonding when water is introduced after contact is made. However, the decrease in the debonding force is much less pronounced than when contact is made in water. The results of Figure 9 indicate that the propensity of water to wet the hydrophilic substrate greatly reduces the interfacial bond between the probe and the PSA and causes debonding at a lower debonding force and without fibrillation.

Both W_{deb} and σ_{max} increase slightly (but systematically) between a 5 and 60 min water immersion for the detachment with the hydrophilic probes. Such an increase is not observed

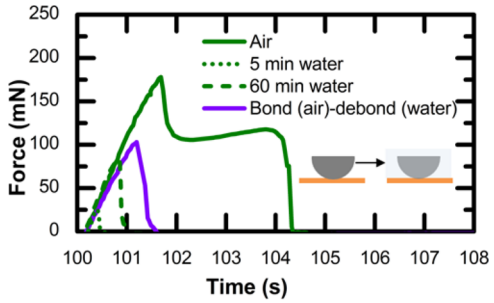

Figure 9. Force–time plots for PSA bonded to piranha-treated glass probe in air. The PSA debonds in air (solid green curve) or in water (dotted green curve, dashed green curve, and purple curve). Measurements are performed after a dwell time of 100 s at 10 mN and a retraction rate of 50 μm/s. For the dotted and dashed green curves, the PSA bonds in water and debonds in water. For the purple curve the PSA bonds in air and debonds in water; DI water is added 45 s before detachment. Internal crack propagation is observed for bonding in air. External crack propagation is observed for bonding in water.

for the hydrophobic probe. We also see a small increase in the PSA–water surface energy between 5 and 60 min immersion obtained from the finger wavelength, which could partly explain this trend. We also know that swelling of a polymer film can lead to an increase in surface energy.[48] Most likely, however, the increase in adhesion for longer immersion time is due to a slightly lower pH[49] of the water with an increase exposure to air in the bath. A higher pH could deprotonate acrylic acid groups. Therefore, lowering of pH from 8 to 6 could lead to stronger hydrogen bonding and weaker electrostatic repulsion thereby causing a stronger adhesion at longer immersion time in water. This reorganization would have a weaker effect on the hydrophobic probe and could explain why we do not see an increase at longer exposure time. Further investigation of the effect of solution conditions such as salt concentration and pH will be performed in a future study.

4. CONCLUSION

We investigated the effect of surface functionalization on the tack of an acrylic PSA submerged in water. To the best of our knowledge, this work is the first systematic investigation of how a water environment affects adhesion forces for PSAs. Using hydrophilic and hydrophobic probes, we find that the PSA tack depends on the surface treatment of the probe in both air and water. Additionally, an important finding is that water does not equally affect the PSA's adhesive strength for high and low surface energy probes. More specifically, the presence of water is more detrimental to the debonding with a hydrophilic probe than with a hydrophobic probe, an observation that cannot be explained based on changing the medium alone. Overall, the intuitive trend emerges in that the PSA tack is stronger in air than in water regardless of surface functionalization, which is consistent with a decrease in van der Waals interactions in water compared to in air.

A key finding includes the observation of different mechanisms for contact formation and relaxation in water compared to in air. Based on images captured during bonding, we identify three types of contact between the PSA and functionalized probe: (I) homogeneous contact formation, (II) multiple distinct circular contact regions that merge with time, and (III) dispersed contact where contact is composed of drainage channels that fade with time. Both hydrophilic and hydrophobic

DOI: 10.1021/acsami.7b13984
ACS Appl. Mater. Interfaces 2017, 9, 42344–42353

probes produce type I contact in air. Hydrophobic probes in water always results in type II contact; however, hydrophilic probes in water make both type II and type III contact. Images captured during debonding allowed us to analyze debonding behavior. Another important finding is that the mode of failure changes depending on the probe and on the environment. For the same PSA we found that debonding in air always occurred via fingering and cavitation. In water, debonding occurred via fingering and cavitation for the hydrophobic probe, while the hydrophilic probe debonded by external crack propagation.

We suspect that trapped or adsorbed water is primarily responsible for the larger adhesive strength differences between contact in air and contact in water. The analysis of bonding and debonding behavior indicates that in water the surface functionalization of the contacting substrate influences both the type of bonding and the debonding mechanism. Analysis of the fingering instability during detachment is indicative of a large increase in the PSA−water surface energy, likely due to reorganization of the functional group at the PSA−water interface.

■ ASSOCIATED CONTENT

Supporting Information

The Supporting Information is available free of charge on the ACS Publications website at DOI: 10.1021/acsami.7b13984.

Detailed Supporting Information detailing the material characterization and image analysis: (1) contact angle and surface energy characterization as well as surface roughness from confocal microscopy; (2) oscillatory rheology for the bulk PSA films upon exposure to water; (3) FTIR-ATR spectra and determination of the water diffusivity in the PSA; (4) in situ fingering image analysis; and (5) force feedback loop under dwell (PDF)

■ AUTHOR INFORMATION

Corresponding Authors

*E-mail: jfrechette@jhu.edu (J.F.)

*E-mail: cabarrios@mmm.com (C.B.)

ORCID

Joelle Frechette: 0000-0001-5680-6554

Notes

The authors declare the following competing financial interest(s): Two of the co-authors are employees of 3M and this work was funded by 3M.

■ ACKNOWLEDGMENTS

This work was supported by 3M and by the National Science Foundation through NSF-CMMI 1728082. We would also like to acknowledge Dr. Georgia Pilkington for help with setting up the initial experiments.

■ REFERENCES

(1) Czech, Z.; Kowalczyk, A.; Kabatc, J.; Świderska, J. Photoreactive UV-crosslinkable solvent-free acrylic pressure-sensitive adhesives containing copolymerizable photoinitiators based on benzophenones. *Eur. Polym. J.* **2012**, *48*, 1446−1454.

(2) Pizzi, A., Mittal, K. L., Eds. *Handbook of adhesive technology, revised and expanded*, 2nd ed.; CRC Press: Boca Raton, FL, 2003.

(3) Wang, T.; Lei, C. H.; Dalton, A. B.; Creton, C.; Lin, Y.; Fernando, K. S.; Sun, Y. P.; Manea, M.; Asua, J. M.; Keddie, J. L. Waterborne, nanocomposite pressure-sensitive adhesives with high tack energy, optical transparency, and electrical conductivity. *Adv. Mater.* **2006**, *18*, 2730−2734.

(4) Rao, M. D. Recent applications of viscoelastic damping for noise control in automobiles and commercial airplanes. *J. Sound Vib* **2003**, *262*, 457−474.

(5) Ahn, B. K.; Kraft, S.; Wang, D.; Sun, X. S. Thermally stable, transparent, pressure-sensitive adhesives from epoxidized and dihydroxyl soybean oil. *Biomacromolecules* **2011**, *12*, 1839−1843.

(6) Creton, C. Pressure-Sensitive Adhesives: An Introductory Course. *MRS Bull.* **2003**, *28*, 434−439.

(7) Creton, C.; Ciccotti, M. Fracture and adhesion of soft materials: a review. *Rep. Prog. Phys.* **2016**, *79*, 046601.

(8) Moon, S.-h.; Foster, M. D. Influence of Humidity on Surface Behavior of Pressure Sensitive Adhesives Studied Using Scanning Probe Microscopy. *Langmuir* **2002**, *18*, 8108−8115.

(9) Schindler, M.; Koller, M.; Muller-Buschbaum, P. Pressure-Sensitive Adhesives under the Influence of Relative Humidity: Inner Structure and Failure Mechanisms. *ACS Appl. Mater. Interfaces* **2015**, *7*, 12319−12327.

(10) Roy, S.; Freiberg, S.; Leblanc, C.; Hore, D. K. Surface Structure of Acrylate Polymer Adhesives. *Langmuir* **2017**, *33*, 1763−1768.

(11) Tan, H. S.; Pfister, W. R. Pressure-sensitive adhesives for transdermal drug delivery systems. *Pharm. Sci. Technol. Today* **1999**, *2*, 60−69.

(12) Nanjundiah, K.; Hsu, P. Y.; Dhinojwala, A. Understanding rubber friction in the presence of water using sum-frequency generation spectroscopy. *J. Chem. Phys.* **2009**, *130*, 024702.

(13) Defante, A. P.; Burai, T. N.; Becker, M. L.; Dhinojwala, A. Consequences of water between two hydrophobic surfaces on adhesion and wetting. *Langmuir* **2015**, *31*, 2398−2406.

(14) Zhang, X.; Myers, J. N.; Bielefeld, J. D.; Lin, Q.; Chen, Z. In situ observation of water behavior at the surface and buried interface of a low-k dielectric film. *ACS Appl. Mater. Interfaces* **2014**, *6*, 18951−18961.

(15) Creton, C.; Hooker, J.; Shull, K. R. Bulk and interfacial contributions to the debonding mechanisms of soft adhesives: extension to large strains. *Langmuir* **2001**, *17*, 4948−4954.

(16) Sherriff, M.; Knibbs, R.; Langley, P. Mechanism for the action of tackifying resins in pressure-sensitive adhesives. *J. Appl. Polym. Sci.* **1973**, *17*, 3423−3438.

(17) Brockmann, W.; Hüther, R. Adhesion mechanisms of pressure sensitive adhesives. *Int. J. Adhes. Adhes.* **1996**, *16*, 81−86.

(18) Benyahia, L.; Verdier, C.; Piau, J. M. The mechanisms of peeling of uncross-linked pressure sensitive adhesives. *J. Adhes.* **1997**, *62*, 45−73.

(19) Verdier, C.; Piau, J. M.; Benyahia, L. Peeling of acrylic pressure sensitive adhesives: cross-linked versus uncross-linked adhesives. *J. Adhes.* **1998**, *68*, 93−116.

(20) Falsafi, A.; Tirrell, M.; Pocius, A. V. Compositional effects on the adhesion of acrylic pressure sensitive adhesives. *Langmuir* **2000**, *16*, 1816−1824.

(21) Sosson, F.; Chateauminois, A.; Creton, C. Investigation of shear failure mechanisms of pressure-sensitive adhesives. *J. Polym. Sci., Part B: Polym. Phys.* **2005**, *43*, 3316−3330.

(22) Wang, Y.; Tan, M. R.; Frechette, J. Elastic deformation of soft coatings due to lubrication forces. *Soft Matter* **2017**, *13*, 6718.

(23) Wang, Y.; Pilkington, G. A.; Dhong, C.; Frechette, J. Elastic deformation during dynamic force measurements in viscous fluids. *Curr. Opin. Colloid Interface Sci.* **2017**, *27*, 43−49.

(24) Wang, Y.; Dhong, C.; Frechette, J. Out-of-contact elastohydrodynamic deformation due to lubrication forces. *Phys. Rev. Lett.* [Online] **2015**, *115*, 248302.

(25) Zosel, A. The effect of fibrilation on the tack of pressure sensitive adhesives. *Int. J. Adhes. Adhes.* **1998**, *18*, 265−271.

(26) Gent, A.; Kim, H. Effect of contact time on tack. *Rubber Chem. Technol.* **1990**, *63*, 613−623.

(27) Davis, C. S.; Lemoine, F.; Darnige, T.; Martina, D.; Creton, C.; Lindner, A. Debonding Mechanisms of Soft Materials at Short Contact Times. *Langmuir* **2014**, *30*, 10626−10636.

(28) Persson, B.; Albohr, O.; Creton, C.; Peveri, V. Contact area between a viscoelastic solid and a hard, randomly rough, substrate. *J. Chem. Phys.* **2004**, *120*, 8779−8793.
(29) Villey, R.; Creton, C.; Cortet, P.-P.; Dalbe, M.-J.; Jet, T.; Saintyves, B.; Santucci, S.; Vanel, L.; Yarusso, D. J.; Ciccotti, M. Rate-dependent elastic hysteresis during the peeling of pressure sensitive adhesives. *Soft Matter* **2015**, *11*, 3480−3491.
(30) Roberts, P.; Pilkington, G. A.; Frechette, J. A multi-mode force microscope for soft matter. *to be submitted*.
(31) Takahashi, K.; Yamagata, Y.; Inaba, K.; Kishimoto, K.; Tomioka, S.; Sugizaki, T. Characterization of Tack Strength Based on Cavity-Growth Criterion. *Langmuir* **2016**, *32*, 3525−3531.
(32) Chiche, A.; Dollhofer, J.; Creton, C. Cavity growth in soft adhesives. *Eur. Phys. J. E: Soft Matter Biol. Phys.* **2005**, *17*, 389−401.
(33) Webber, R. E.; Shull, K. R.; Roos, A.; Creton, C. Effects of geometric confinement on the adhesive debonding of soft elastic solids. *Phys. Rev. E: Stat. Phys., Plasmas, Fluids, Relat. Interdiscip. Top.* [Online] **2003**, *68*, 021805.
(34) Acres, R. G.; Ellis, A. V.; Alvino, J.; Lenahan, C. E.; Khodakov, D. A.; Metha, G. F.; Andersson, G. G. Molecular structure of 3-aminopropyltriethoxysilane layers formed on silanol-terminated silicon surfaces. *J. Phys. Chem. C* **2012**, *116*, 6289−6297.
(35) Basabe-Desmonts, L.; Beld, J.; Zimmerman, R. S.; Hernando, J.; Mela, P.; García Parajó, M. F.; van Hulst, N. F.; van den Berg, A.; Reinhoudt, D. N.; Crego-Calama, M. A simple approach to sensor discovery and fabrication on self-assembled monolayers on glass. *J. Am. Chem. Soc.* **2004**, *126*, 7293−7299.
(36) Bhattacharya, S.; Datta, A.; Berg, J. M.; Gangopadhyay, S. Studies on surface wettability of poly (dimethyl) siloxane (PDMS) and glass under oxygen-plasma treatment and correlation with bond strength. *J. Microelectromech. Syst.* **2005**, *14*, 590−597.
(37) Kowalski, A.; Czech, Z.; Byczyński, Ł. How does the surface free energy influence the tack of acrylic pressure-sensitive adhesives (PSAs)? *J. Coating Tech Res.* **2013**, *10*, 879−885.
(38) Deplace, F.; Carelli, C.; Mariot, S.; Retsos, H.; Chateauminois, A.; Ouzineb, K.; Creton, C. Fine tuning the adhesive properties of a soft nanostructured adhesive with rheological measurements. *J. Adhes.* **2009**, *85*, 18−54.
(39) Roberts, A. Squeeze films between rubber and glass. *J. Phys. D: Appl. Phys.* **1971**, *4*, 423−432.
(40) Nase, J.; Lindner, A.; Creton, C. Pattern formation during deformation of a confined viscoelastic layer: From a viscous liquid to a soft elastic solid. *Phys. Rev. Lett.* [Online] **2008**, *101*, 074503.
(41) Ghatak, A.; Chaudhury, M. K. Adhesion-induced instability patterns in thin confined elastic film. *Langmuir* **2003**, *19*, 2621−2631.
(42) Lakrout, H.; Sergot, P.; Creton, C. Direct observation of cavitation and fibrillation in a probe tack experiment on model acrylic pressure-sensitive-adhesives. *J. Adhes.* **1999**, *69*, 307−359.
(43) Ganghoffer, J.; Schultz, J. An analytical model of the mechanical behaviour of elastic adhesively bonded joints. *J. Adhes.* **1996**, *55*, 285−302.
(44) Saffman, P. G.; Taylor, G. The penetration of a fluid into a porous medium or Hele-Shaw cell containing a more viscous liquid. *Proc. R. Soc. London, Ser. A* **1958**, *245*, 312−329.
(45) Paterson, L. Radial fingering in a Hele Shaw cell. *J. Fluid Mech.* **1981**, *113*, 513−529.
(46) Good, R. J. Contact angle, wetting, and adhesion: a critical review. *J. Adhes. Sci. Technol.* **1992**, *6*, 1269−1302.
(47) Israelachvili, J. N. *Intermolecular and surface forces*, 3rd ed.; Academic Press: London, U.K., 2015.
(48) Sedev, R.; Petrov, J.; Neumann, A. Effect of swelling of a polymer surface on advancing and receding contact angles. *J. Colloid Interface Sci.* **1996**, *180*, 36−42.
(49) Wang, T.; Canetta, E.; Weerakkody, T. G.; Keddie, J. L.; Rivas, U. pH dependence of the properties of waterborne pressure-sensitive adhesives containing acrylic acid. *ACS Appl. Mater. Interfaces* **2009**, *1*, 631−639.

DOI: 10.1021/acsami.7b13984
ACS Appl. Mater. Interfaces 2017, 9, 42344−42353